Interaction of Melt Spinning and Drawing Variables on the Crystalline Morphology and Mechanical Properties of High-Density and Low-Density Polyethylene Fiber

JAMES L. WHITE, KHUSHAL C. DHAROD, and EDWARD S. CLARK, *Department of Chemical and Metallurgical Engineering, The University of Tennessee, Knoxville, Tennessee 37916*

Synopsis

An experimental study of the spinnability and the variation in crystallinity and orientation in high-density and low-density polyethylene fibers with melt spinning and drawing conditions has been carried out. Three polymers (two high-density and one low-density) and eicosane ($C_{20}H_{42}$) were studied. The maximum spinnability was in the lower molecular weight high-density polyethylene. Hermans-Stein a, b, and c crystallographic axis orientation factors were computed from wide-angle x-ray scattering patterns. In the spun fiber, small take-up velocities cause the b axis to become perpendicular to the fiber axis in each fiber. The c axis increasingly orients itself parallel to the fiber axis as take-up velocity increases. The a axis orientation is different for each polymer. The results are interpreted in terms of modern theories of crystalline morphology, specifically the development of row structures. In the drawing experiments, the two high-density polyethylenes necked. A phenomenological theory of necking is discussed. The a, b, and c axis orientation factors were determined for different stages of drawing. In the necked regions and in completely drawn fibers, the c axis was parallel to the fiber axis and the a and b axes are perpendicular to the fiber axis. The tangent Young's modulus and tensile strength of the spun fibers increased with take-up velocity and in the drawn fibers were an order of magnitude higher than in the spun fiber. The mechanical properties of spun fiber may be correlated with the c axis (Hermans) orientation factor. The drawn fiber shows significant variations in Young's modulus and tensile strength at constant unit cell orientation.

INTRODUCTION

The production of fibers from polymer melts generally involves two steps. First, melt is extruded producing a vertical descending thread which is cooled in transit and taken up on a godet in solidified form. This process is known as *melt spinning*. The spun fiber is then subjected to a second operation in which it is unwound from a slow roll, stretched (drawn) under controlled temperature conditions, and taken up on a fast roll. This second process is known as *drawing*. A wide range of spinning and drawing variables is available to the fiber manufacturer. The choice is one not to be taken lightly or completely on the basis of economic considerations for the

2539

crystalline character, and mechanical properties can vary considerably depending upon the decision reached.

The melt spinning and subsequent drawing of synthetic fibers were devised by Carothers and his colleagues[1-3] in 1932–33. Most pertinent features of the influence of melt spinning and drawing variables were noted by Carothers and Hill,[1] including the effect of take-up velocity on crystalline orientation and mechanical properties, the development of necks during drawing, and the different crystalline orientations in the necked and unnecked fibers. Since this work, numerous researchers[4-17] have investigated the influence of melt spinning variables on the orientation and crystalline character of fibers, and there has also been an effort to investigate the drawing of filaments.[18-26] Research on drawing has mainly dealt with four specific types of polymers: polyethylene, polypropylene, nylons 6 and 66, and poly(ethylene terephthalate) (PET), the latter three being important synthetic fibers. Despite the number of studies noted above on melt spinning and filament stretching, few are of quantitative nature, and an even smaller number deal with the interaction of melt spinning and drawing variables.

In recent years, The University of Tennessee has developed a research program on the melt spinning and drawing of fibers.[16,18,27-29] The early work emphasized rheological and heat transfer phenomena in the spinline.[27,28] In turning to structure development in spinning and drawing, it was decided to begin our melt spinning studies using polymers which formed simple crystallographic structure and exhibited minimal polymorphism. Polymorphism, moisture-influenced crystallization rates, poor x-ray patterns, and low unit cell symmetries ruled out nylon, polyester, and polypropylene for the initial studies. Abbott and White[16] were led to choose polyethylene with its orthorhombic unit cell as a starting point and determined crystallinity level and the Herman-Stein[30-31] orientation factors as a function of spinning conditions. In a later study, Dees and Spruiell[18] determined the variation in level of crystallinity and orientation factors in polyethylene with position along the spinline. In this paper, we will be concerned with the interrelationship between the melt spinning and drawing variables on the nature of the crystallinity and molecular orientation and in turn their influence on the mechanical properties.

SPECIFICATION OF FIBER STRUCTURE

Polyethylene fibers possess a complex structure. As viewed from a macroscopic level, they are a crystalline material which x-ray data identifies as orthorhombic.[20,33] However, direct measurements of crystallinity[32,34] by x-ray diffraction, density, etc., yield values considerably less than 100% and, in certain low-density "branched" polyethylenes, values of less than 25%. Whatever crystalline superstructures exist must possess significant disorder on a smaller scale. In any case, the level of crystallinity measured may be interpreted as a level of order. In this paper, we will be determining this gross overall crystallinity level in fibers as func-
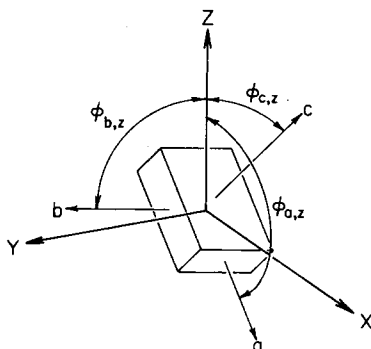
Fig. 1. Orientation of unit cell at polyethylene.

tion of spinning and drawing variables by density and calorimetric techniques. The interpretation of these data in terms of specific relationships between the level of order in molecular arrangements and process variables is not unique and is dependent on the detailed structural model chosen.

A second major structural feature of polyethylene fibers is the level of orientation of the polyethylene molecules and of the crystalline material relative to the fiber axis. Hermans and his co-workers[30] (compare Ziabicki[35]) have proposed a measure of the average orientation of polymer chains relative to the axis of a fiber in which there is complete molecular symmetry around the axis. The Hermans orientation factor is

$$f_{\mathrm{H}} = \frac{\alpha_{\|} - \alpha_{\perp}}{\alpha_1 - \alpha_2} \qquad (1)$$

where $\alpha_{\|}$ and $\alpha_{\perp}$ are the average polarizabilities parallel and perpendicular to the fiber axis and α_1 and α_2 are the polarizabilities along and perpendicular to the polymer chain. If the polymer chains are envisaged to occur as rigid rods in a rigid crystallite, then Hermans et al. show

$$f_{\mathrm{H}} = {}^1/_2[3 \ \overline{\cos^2\Phi_{c,z}} - 1] \qquad (2)$$

where $\Phi_{c,z}$ is the angle between the polymer chain axis and the fiber axis and the bar over $\cos^2\Phi_{c,z}$ indicates on averaging over all crystallites around the solid angle. For the case of complete parallel alignment of chains with the fiber axis, $\Phi_{c,z}$ is zero and f_{H} becomes unity. For the case of chains aligned perpendicular to the fiber axis, $\Phi_{c,z}$ is 90°, and f_{H} is -0.5. Stein[31] has pointed out that eq. (2) may be generalized so as to include all three crystallographic axes,

$$f_a = {}^1/_2[3 \ \overline{\cos^2\Phi_{a,z}} - 1] \qquad (3a)$$

$$f_b = {}^1/_2[3 \ \overline{\cos^2\Phi_{b,z}} - 1] \qquad (3b)$$

$$f_c = {}^1/_2[3 \ \overline{\cos^2\Phi_{c,z}} - 1] \qquad (3c)$$

where $\Phi_{a,z}$, $\Phi_{b,z}$ and $\Phi_{c,z}$ (defined by Figure 1) represent the angles formed by the a, b, and c crystallographic axes. The c axis orientation factor

corresponds to the Hermans orientation factor.   For an orthorhombic unit cell such as exists in polyethylene, Stein[31] shows that the orthogonality requires

$$f_a + f_b + f_c = 0. \qquad (4)$$

It is to be noted that the three orientation factors of eq. (3) specify orientation in the well-ordered regions of the fiber and not in the amorphous regions (see the discussions of Stein and Norris[36] and Samuels[24,37]).   Secondly this function specifies only the averaged orientation of the various crystallites but not their distribution.   More than one distribution of crystallites (morphology) may produce the same orientation factors.

In this paper, we will describe the structure of polyethylene fibers in terms of a crystallinity index which represents a measure of the average order within the polymer in addition to the three Hermans-Stein crystalline orientation factors which measure the average position of the three crystallographic axes relative to the fiber axis.   Such a specification is incomplete and in fact says relatively little about the actual arrangements of polymer chains or the type of order on a level higher than the unit cell.   It is well known that ordered structure on a higher level exists.   Small-angle x-ray diffraction shows repeat distances of 100–200Å [11,23,38] in both oriented and unoriented polymer.   Numerous papers discuss qualitative aspects of spherulitic structure[20,39,40] and the fibrils which result from drawing experiments.[23,25]

The orientation factors which we measure experimentally from fiber patterns are averaged in another sense.   There is no reason to expect that fibers will be structurally uniform across their cross section.   There is indeed evidence which suggests otherwise.   The fibers which are formed from a descending molten thread solidify radially from the outer surface inward.[41]   The outer layers will crystallize under a condition of high stress and will possess a highly oriented structure.   As crystallization proceeds inward from the surface, the continuity of the solid skin–molten core structure requires that the core will crystallize under less stress than the surface.   With the solid skin supporting the load, the molecular rearrangement in the melt can relieve much of the stress, with resultant lower orientation in the core during solidification.   One would thus expect the internal portions of a fiber to possess a lower orientation than the external layer. Radial variations in structure of fibers have been noted by scanning electron microscopy[42] and by optical microscopy,[43] with the surface layers appearing most highly oriented.   Fung and Carr[13] have shown that melt-spun polyethylene fibers exhibit a radial variation of birefringence, with the maximum birefringence found at the outer edge of the fiber.   Katayama, Amano, and Nakamura[11] and Dees and Spruiell,[18] who give the above argument about fiber solidification, have observed that the crystalline c axis orientation factor in the crystallizing fiber in a spinline decreases with increasing distance from the spinneret concurrent with the increase in overall crystallinity.

EXPERIMENTAL

Materials

Three commercial polyethylenes and a paraffin were investigated in this study. Two of the polymers were of the high-density type, one made by Dow Chemical with a melt index of 6.0 and a second manufactured by Phillips Petroleum with a melt index of 0.1. The third polyethylene was a low-density type manufactured by Dow Chemical with melt index of 5.0. The paraffin was eicosane ($C_{20}H_{42}$) obtained from Fischer Chemical. The three polymers will be designated in the remainder of the paper as HMW-HDPE = high-density polyethylene (Ml = 0.1); LMW-HDPE = high-density polyethylene (Ml = 6.0); and LDPE = low-density polyethylene. The HMW-HDPE and LMW-HDPE represent high molecular weight and low molecular weight high-density polyethylene.

Rheological Measurements

As all melt spinning experiments were carried out at 180°C, the rheological properties of the melts studied were investigated at that temperature. An Instron capillary rheometer was used to perform the measurements. The viscosity was computed using standard methods.[44,45]

Melt Spinning

The various polyethylenes were melt spun from an Instron capillary rheometer at 180°C. The melt was then forced through a capillary having a diameter of 0.0543 in. and an L/D ratio of 20.0. The extruded filament was taken up on a bobbin at predetermined speeds. The spinning path for the taken-up fiber was approximately 90 cm. The mass flow rate was the same for all experiments and was approximately 3.25 g/min. The take-up speeds ranged up to 453 meters/min. It is to be noted that the geometry of the spinline prevents the fibers from being spun vertically downward.

Cold Drawing

The spun fibers were drawn in an Instron tensile testing machine at room temperature at a cross-head speed based upon a drawing rate of 20% of the initial fiber gauge length per minute.

X-Ray Diffraction

Wide-angle x-ray diffraction patterns were used to determine crystalline orientation factors. Specifically the (200) and (020) crystallographic plane orientations were used to determine f_a and f_b, and eq. (4) was used to obtain f_c. A fixed geometric relationship exists between the angles $\Phi_{a,z}$, $\Phi_{b,z}$, the Bragg angle θ, and the angle ψ (azimuthal angle between
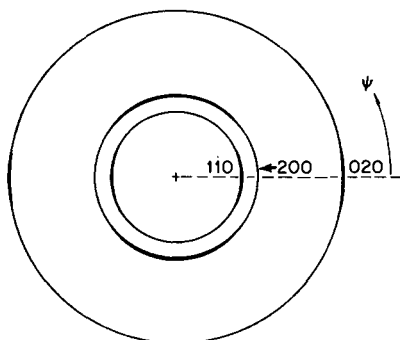
Fig. 2. Definition of angle ψ on wide-angle x-ray scattering pattern for polyethylene.

the equator and the observed position of diffraction on the flat plate fiber pattern, see Fig. 2). Specifically (see Stein[31]),

$$\overline{\cos^2\Phi_{a,Z}} = \cos^2\theta_a \overline{\sin^2\psi_a} \tag{5a}$$

$$\overline{\cos^2\Phi_{b,Z}} = \cos^2\theta_b \overline{\sin^2\psi_b} \tag{5b}$$

where

$$\overline{\sin^2\psi} = \frac{\displaystyle\int_0^{\pi/2} I(\psi) \sin^2\psi \cos\psi \, d\psi}{\displaystyle\int_0^{\pi/2} I(\psi) \cos\psi \, d\psi} \tag{6}$$

where $I(\psi)$ is the relative intensity of the diffracted beam at angle ψ.

A Rigaku General Electric rotating-anode, high-intensity x-ray unit was used to obtain the diffraction patterns on the polyethylene fibers. This allowed determination of fiber patterns in a period of about 13 min.

Density

Densities of the spun and drawn fibers were determined with a density gradient column constructed using distilled water and isopropyl alcohol according to the method described by Tung and Taylor.[46] A crystallinity index was calculated as a percentage based on measured densities of the fibers using the relationship

$$X = \frac{V_a - V}{V_a - V_c} \tag{7}$$

where V is the reciprocal of the measured density and V_a and V_c are Swan's expressions[47] for the specific volume of the amorphous and crystalline fractions. However, one must be wary of the existence of voids in the fibers which will introduce inaccuracies into eq. (7).

Calorimetry

The crystallinity of the spun and drawn fibers was also determined using a Perkin-Elmer differential scanning calorimeter Model N. DSG-18. The
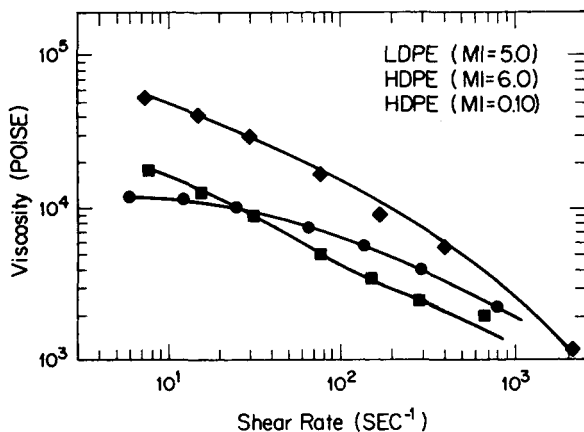
Fig. 3. Non-Newtonian viscosity function of the LMW-HDPE, HMW-HDPE, and the LDPE at 180°C.

heat of fusion for a known mass of sample was determined from the area under the fusion portion of the trace determined at 10°C/min. This was compared with a heat of fusion of 66.2 calories/g which was taken to be the value for a perfect crystal.

Mechanical Properties

Force–elongation data for the spun and drawn fibers were obtained using an Instron tensile testing machine Table Model-TM with hydraulic action grips. An elongation rate of 100%/min was used.

RHEOLOGICAL PROPERTIES

Figure 3 contains a plot of the non-Newtonian viscosity functions μ of the three polyethylene melts as a function of shear rate. The higher
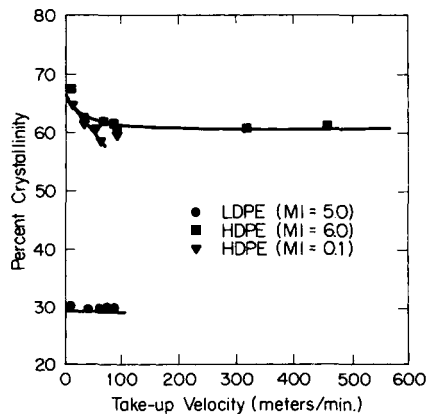
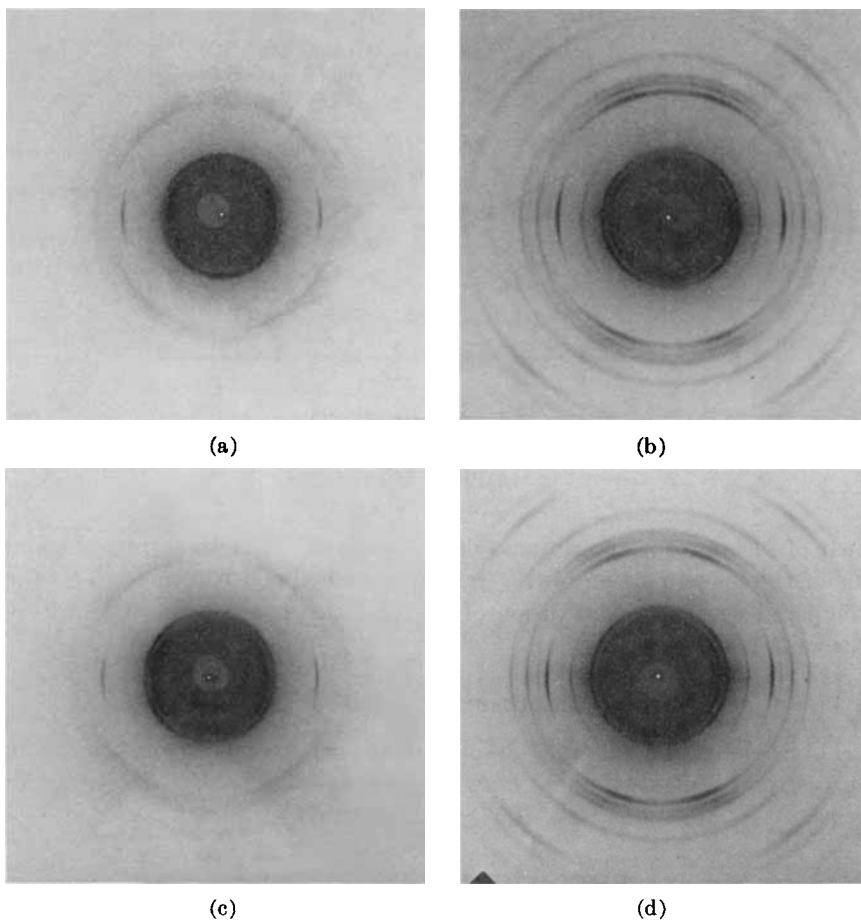Fig. 4. Crystallinity of polyethylene fibers as a function of take-up velocity.

(a)

(b)

(c)

(d)

Fig. 5 *(continued)*

viscosity level of the HMW-HDPE is apparent. The parallelism of the viscosity–shear rate curves for the two high-density polyethylenes is of interest. The LDPE exhibits a greater degree of non-Newtonian character than the high-density polyethylenes.

MELT SPINNING

Results

The spinnability (i.e., the ability to spin fibers from the melt without spinline breakage) of the three polymers considered in this study were rather different. The HMW-HDPE and LDPE could be taken up with velocities only to about 80 meters/min, while LMW-HDPE could be taken up at rates to about 450 meters/min. The HMW-HDPE was slightly more spinnable than the LDPE. It was not possible to spin the eicosane into fibers, even at temperatures just above its melting point.
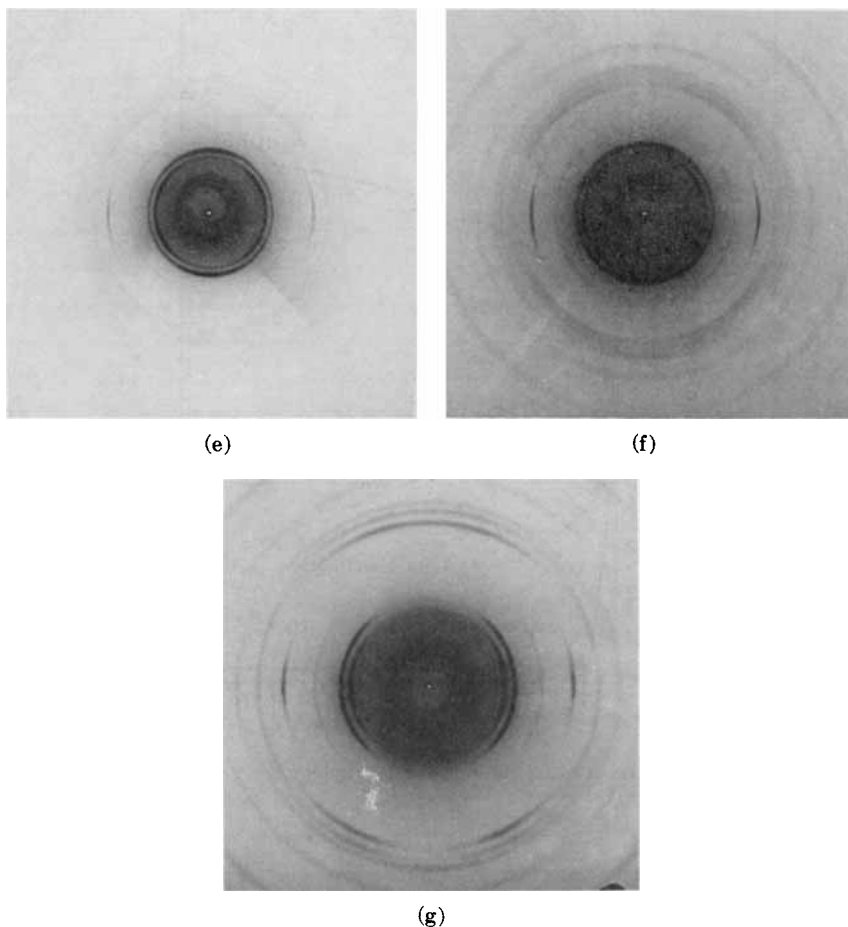
Fig. 5. Wide-angle x-ray scattering patterns of polyethylene fibers at different take-up velocities. (a) Take-up velocity = 37 m/min (LDPE); (b) take-up velocity = 37 m/min (HMW HDPE); (c) take-up velocity = 80 m/min (LDPE); (d) take-up velocity = 80 m/min (HMW HDPE); (e) take-up velocity = 37 m/min (LMW HDPE); (f) take-up velocity = 80 m/min (LMW HDPE); (g) take-up velocity = 455 m/min (LMW HDPE).

The level of crystallinity of the three polyethylene fibers is shown as a function of take-up velocity in Figure 4. Crystallinities obtained from density and calorimetry measurements were found generally to agree within about 2%. The crystallinity is found to decrease at first with increasing take-up velocity for the LMW-HDPE and the HMW-HDPE, but the overall level of crystallinity in the latter polymer is lower. The level of crystallinity in the LMW-HDPE, however, rapidly reaches a lower asymptote. The behavior of LDPE is strikingly different. Its level of crystallinity is much lower (~30%) than the two HDPEs (~65%) and, unlike them, is independent of take-up velocity.
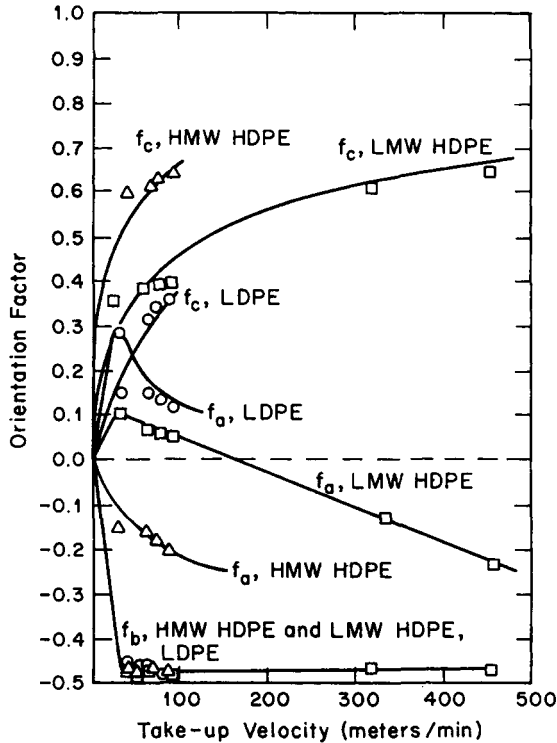
Fig. 6. The a, b, c, axis orientation factors for polyethylene fibers as a function of take-up velocity.

Figure 5 contains a series of wide-angle x-ray scattering patterns showing the development of crystalline orientation for the LMW-HDPE, HMW-HDPE, and LDPE. Figure 6 plots the three crystallographic orientation factors as a function of take-up velocity for the three polyethylenes studied. It is apparent that for all three polymers, the b crystallographic axis orients itself perpendicular to the fiber axis at the lowest take-up velocities. There is also tendency towards c axis orientation with increasing take-up velocity. The tendency is the strongest in the HMW-HDPE and the weakest in the LDPE. The maximum value the c axis orientation factor attains is about 0.6. The LDPE and, to a lesser extent, the LMW-HDPE show a tendency toward a axis orientation at low take-up velocities. However, as the take-up velocity for the LMW-HDPE is increased, the a axis orientation decreases, and becomes random and eventually perpendicular to the fiber axis. For the LDPE, a axis orientation decreases with increasing take-up velocity, but f_a still remains positive.

DISCUSSION

If we combine our observations of spinnability of polyethylene melts together with those of Abbott and White[16] and Ziabicki and Kedzierska,[7]

it is apparent that if one considers the variation in spinnability with molecular weight of n-paraffins, one finds that neither very low nor very high molecular weight polymer may be spun from an extruder into fiber. There will be a maximum in the spinnability–molecular weight curve. The LMW-HDPE is nearer the maximum than the HMW-HDPE. These results agree with the data on other polymer systems. Carothers and Van Natta[2] found that linear polyesters from ω-hydroxydecanoic acid could only be spun into fiber at molecular weights of 10,000 and above. Ziabicki,[10] in summarizing data from the literature, found a maximum in the dependence of spinnability upon molecular weight. Certainly, the lowest molecular filaments break by the Rayleigh surface tension instability.[48,49] At higher molecular weights, the higher viscosity damps out the disturbance leading to enhanced stability. Here any analysis must consider the interaction of ductile yielding during stretching as well as surface tension (see Tomotika[50] and Pearson and Matovich[51]). The development of viscoelasticity at high molecular weights should also lend to the stability.[52] At still higher molecular weights, brittle fracture resulting from energy storage will lead to failure.[53] These ideas are in general accord with those of Ziabicki.[10]

The decreasing level of crystallinity in high-density polyethylene with increasing take-up velocity agrees with the results of Abbott and White[16] and Dees and Spruiell.[18] Two views of the meaning of such crystallinity variations seem possible. Ziabicki[10] (see also Abbott and White[16]) suggests that it is the result of increased cooling rates due to the higher ratio of surface area to mass in the fiber at the high take-up velocities which leads to a smaller residence time in the region of maximum crystallization rates. While this seems reasonable for fibers with glass transition temperatures above room temperature, it would seem questionable for polyethylene which crystallizes almost infinitely rapidly at temperatures not too far below its melting temperature. We can offer an alternate view which perhaps is more useful. There seem to be no amorphous regions in high-density polyethylene in the classical sense. Indeed, Dees and Spruiell[18] show that birefringence orientation is almost completely due to crystalline orientation. Application of tensile stress greatly increases the rate of crystallization, which in turn gives rise to greater levels of crystalline disorder. There is insufficient time for conformational adjustment of the chains to produce the high level of order often found in single crystals carefully grown from solution. Thus, we suggest that a lower crystallinity is primarily a result of increased crystallization rate. In the latter part of the paper, we will discuss possible detailed morphologies consistent with this interpretation.

From inspecting the plots of the orientation factors versus take-up velocity, it would seem that each of the three melts exhibits different characteristics. For the LMW-HDPE, there are three distinct regions. At the lowest take-up velocity, there is no preferred orientation and

$$f_a = f_b = f_c = 0. \tag{8a}$$

As the take-up velocity increases, f_b becomes negative and f_a and f_c become positive and approximately equal, i.e.,

$$f_b \sim -0.45 \qquad f_a \sim f_c \sim 0.22. \qquad (8b)$$

It has been pointed out by Spruiell[54] that these are nearly the exact values for the type of orientation in which the b axis is prependicular to the fiber axis, with the a and c axes randomly disposed within a plane parallel to the fiber axis. This assignment is based on the sum of the three orientation functions being zero, eq. (4), with $f_b = -0.5$ and equality of f_a and f_c. An alternate assignment of orientation satisfying Eq. (8b) would be one in which the b axis was normal to the fiber axis with a and c axes each inclined 45° to the fiber axis. The implications of these solutions to morphology will be discussed later. At the higher take-up velocities, it is found that

$$f_b = -0.45 \qquad f_a \rightarrow -0.20 \qquad f_c \rightarrow 0.65. \qquad (8c)$$

The a axis as well as the b crystallographic axis tends to become perpendicular to the fiber axis. The c axis, i.e., the polymer chains themselves, becomes increasingly parallel to the fiber axis.

For the HMW-HDPE, we find eq. (8a) to be valid at the lowest take-up velocities. However, on increasing the take-up velocity, the b axis immediately becomes perpendicular to the fiber axis, and the a axis shows a lesser tendency to orient perpendicular to the fiber axis. Thus, one moves directly into the region defined by eq. (8c) without apparently ever exhibiting the behavior defined by eq. (8b). However, this might be due to our not having fibers produced at very low take-up speeds.

The LDPE behavior shows greater differences. While eq. (8a) remains valid at very low take-up speeds, one finds a combination of the b axis rapidly becoming perpendicular to the fiber axis with a strong tendency for the a axis to become parallel to the fiber axis. At the highest take-up velocity:

$$f_b \sim -0.45 \qquad f_a \sim 0.1 \qquad f_c \sim 0.35 \qquad (8d)$$

which still indicates considerably more a axis orientation than found in eq. (8c).

These observations are in general agreement with earlier studies of melt spun polyethylene fibers by Katayama, Amano, and Nakamura,[11] Kitao, Ohya, Furukawa, and Yamashita,[14] Abbott and White,[16] and Dees and Spruiell.[18] The three latter groups clearly observed the eq. (10a)–(10b)–(10c) transformation. The higher levels of a axis orientation in low-density than in higher-density polyethylenes were observed by Abbott and White. A reinspection of their fiber patterns of the high-density polyethylenes also indicates that the maximum c axis orientation factor achievable seems to be about 0.6.

DRAWING

Results

The drawability, i.e., the ability to elongate the fibers without breakage, of the three melt-spun polyethylenes varied considerably. The LDPE
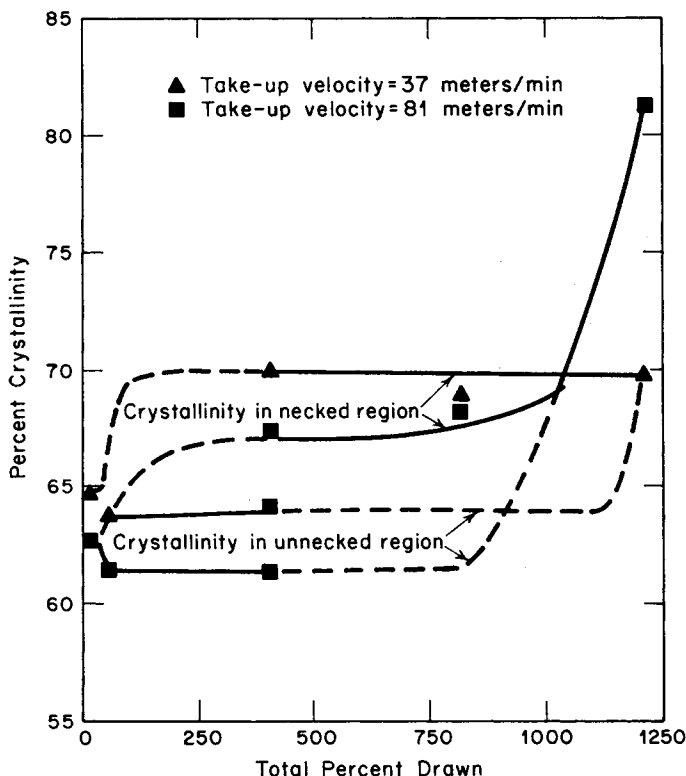
Fig. 7. Variation in crystallinity of LMW-HDPE with extent of draw for fibers drawn to different extents.

fibers broke short, whereas the HMW-LDPE and the LMW-HDPE could be stretched to high draw ratios. We define draw ratio and per cent draw by

$$\text{DR} = \frac{L_f}{L_0} \qquad \text{per cent draw} = \frac{L_f - L_0}{L_0} \times 100 \qquad (9)$$

where L_0 is the initial fiber length and L_f is its final length. The LDPE fibers spun at 37 meters/min can be stretched to DR values of 2.5–3.5 before breakage, while the LMW-HDPE spun under the same conditions could be stretched beyond a draw ratio of 20 and the HMW-HDPE beyond a draw ratio of 12. The extent of draw before break decreases with increasing fiber take-up velocity. The DR to break for the LMW-HDPE decreases from a value greater than 20 for a take-up velocity of 37 meters/min to 7–10 for a take-up velocity of 455 meters/min.

In the LMW-HDPE and the HMW-HDPE (but not the LDPE), necks and shoulders were observed to form during the cold-drawing operation. The DR required for disappearance of necks and shoulders in the two HDPE samples was found to depend upon take-up velocity during melt spinning. For LMW-HDPE spun at 37 meters/min, a draw ratio of 13
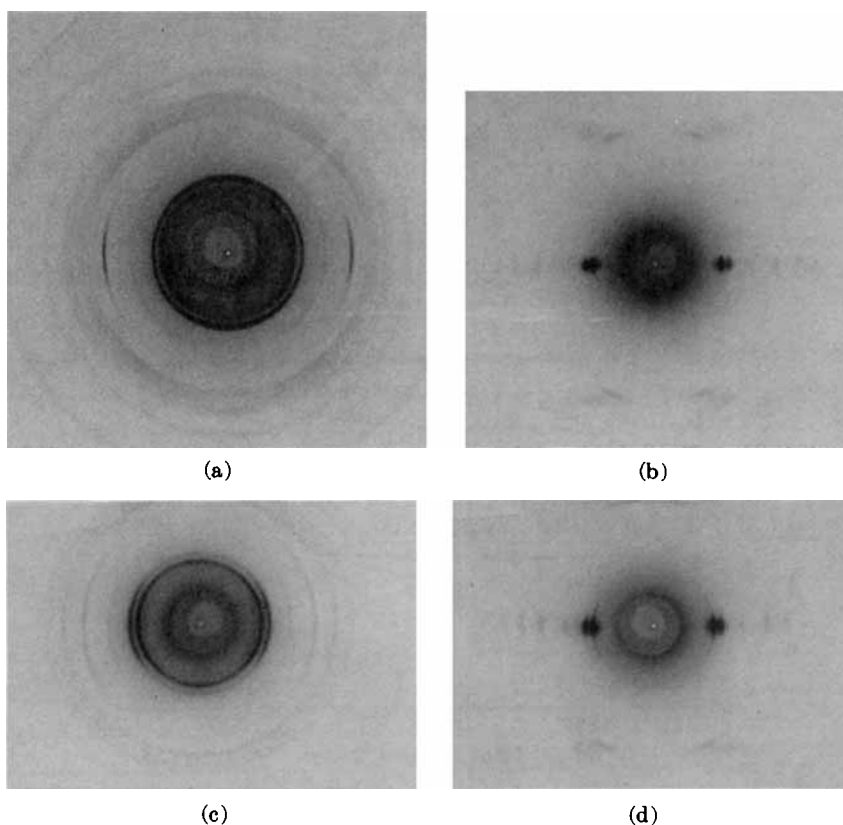
Fig. 8. X-Ray diffraction patterns for drawn polyethylene fibers. (a) Diffraction pattern of spun HDPE (MI = 6.0) fiber, take-up velocity = 81 m/min; (b) diffraction pattern of drawn HDPE (MI = 6.0) fiber, take-up velocity = 81 m/min, draw ratio = 13 (necks and shoulders being absent); (c) diffraction pattern of unnecked region of drawn HDPE (MI = 6.0) fiber, take-up velocity = 81 m/min, total draw ratio = 5; (d) diffraction pattern of necked region of drawn HDPE (MI = 6.0) fiber, take-up velocity = 81 m/min, total draw ratio = 5.

was required to make the necks disappear, while for a fiber spun at 450 meters/min, a draw ratio of only 7 was required. During the drawing of the two HDPE's, "whitening" occurs in the necked regions which is accompanied by a large drop in density. This would imply the formation of voids. Generally, differential scanning calorimeter crystallinities were higher in the necked regions than the unnecked portions of the fibers, while density crystallinities were much lower. We have accepted the former values throughout the remainder of this section.

Figure 7 plots the variation of the crystallinity in the LMW-HDPE with extent of draw for fibers with varying take-up velocities. The LMW-HDPE curves may be seen to be double valued and to converge to single points at a high draw ratio where the necks disappear. As mentioned
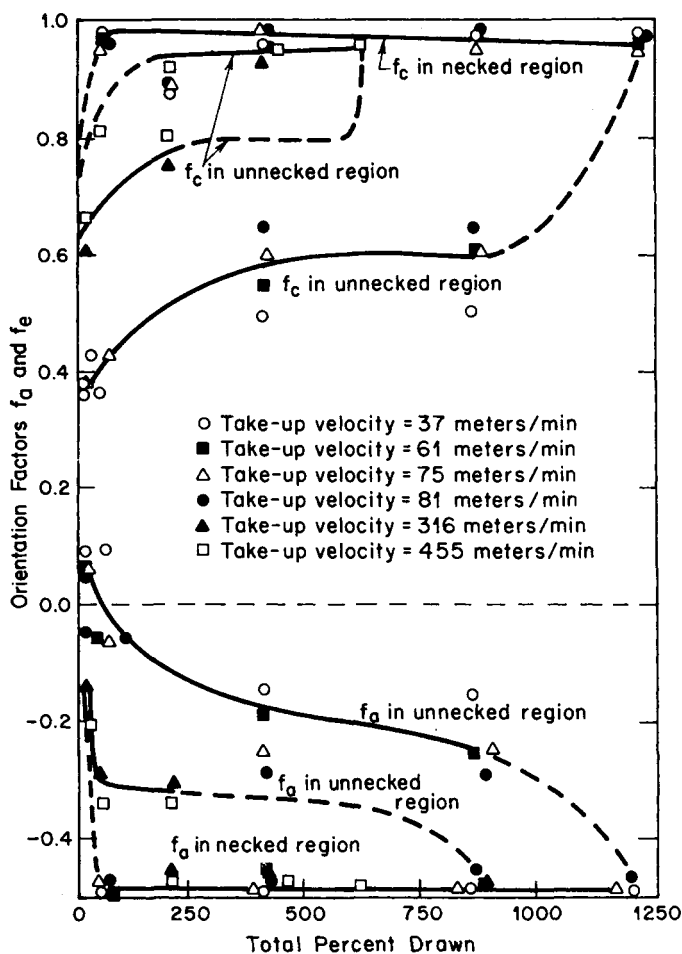
Fig. 9. Orientation factors f_c and f_a in necked and unnecked regions of LMW-HDPE fiber as a function of spinning conditions.

above, the crystallinities are generally higher in the necked than the unnecked regions.

Figure 8 contains x-ray diffraction patterns for the drawn polyethylene fibers for varying draw ratios. The increased level of c axis orientation parallel to the fiber axis and a axis orientation perpendicular to the fiber axis in the final drawn fibers is apparent. The higher degree of this type of orientation in the necked as compared with the unnecked regions should also be apparent. The two Hermans-Stein orientation factors f_a and f_c were determined from the fiber patterns and are plotted as a function of draw ratio in Figures 9 and 10 (f_b not contained in these plots is of order -0.5). The orientation factor curves are double valued after necks appeared. In the unnecked region, f_a and f_c are functions of the initial take-up velocity, f_c being an increasing function of take-up velocity. In the necked regions, f_c has a value of 0.95 or greater, and f_a is of order -0.45.
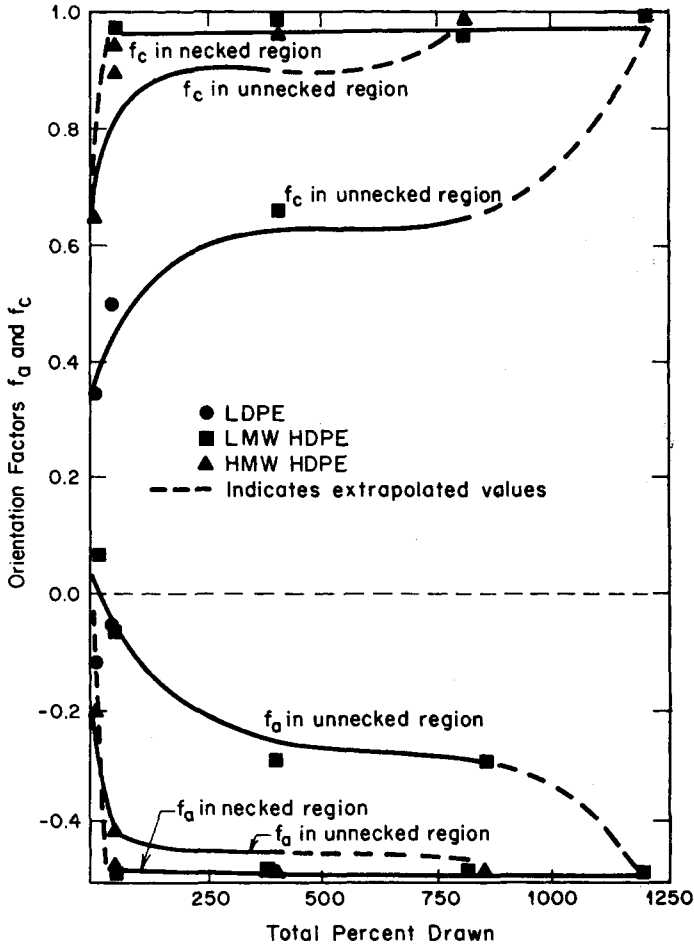
Fig. 10. Orientation factors f_c and f_a of different polyethylene drawn fibers in necked and unnecked regions.

Discussion

The question as to the mechanism leading to the formation and propagation of necks must be faced. We begin with the point that materials of varying structure exhibit necking.[1,19,21] From a phenomenologic viewpoint, it must be due to existence of geometric or material nonhomogeneities in the fiber. In an industrial drawing operation, a heated plate or tube is used to induce material nonuniformity and induce necking at a particular spatial position. However, in our experiment, no such nonhomogeneities exist, and the cause must be geometric defects, i.e., necking probably begins at cross sections possessing higher concentrations of flaws. If this is the origin of necking, we must add to the above discussion the mechanism of neck propagation. Once a neck is formed, why does it not either

disappear or grow catastrophically as in a metal? The answer must lie in the shape of the stress–strain curve; specifically, the material must exhibit something anologous to "strain hardening," i.e., the resistance to strain increases with increasing draw ratios. The higher orientations and levels of crystallinity in the necked regions support this interpretation. Additional support comes from the mechanical property measurements described in the next section.

Some question exists as to the meaning of the crystallinity data in Figure 7, for during the temperature upsweep the samples are annealed and some "healing" or rearrangement of the crystalline structure occurs. The level of this annealing will certainly vary with the degree of orientation, and there are considerable differences in orientation between the necked and the unnecked regions.

From studying the LMW-HDPE and HMW-HDPE orientation factor plots, it is apparent that in the necked regions, and in the drawn fibers after the disappearance of soulders and necks,

$$f_b \sim -0.45 \qquad f_a \sim -0.45 \qquad f_c \sim 0.9\text{–}1.0 \tag{10}$$

which indicates nearly uniform axial crystalline orientation. This represents a fourth region of distribution of orientation factors for processed high-density polyethylene fibers, in addition to eqs. (8a), (8b), and (10d).

There is an enormous literature on stretching spherulitic polyethylene films and fibers. What comparisons are possible would seem in general agreement with our work. However, a wide variety of drawing rates, temperatures, and polyethylene types have been used which make specific comparison difficult. Our low-density polyethylene fibers did not neck. However, there have been numerous studies of stretched polymers of this type using varying conditions which apparently do lead to necking.

MECHANICAL PROPERTIES

General Considerations

The melt-spun fibers were subjected to uniaxial stretching by a cross head moving at constant velocity. The response of the fibers to the applied deformation is in general complex. Many fibers, for example, exhibit formation and growth of necks under these conditions, as was seen in the discussion of the previous section. The crystalline orientation of the material in the necked regions differs considerably from that in the remainder of the fiber. This complex response does not allow ready interpretation of the deformation behavior in terms of any well-established area of deformation mechanics. We shall proceed by plotting the data in terms of stress σ and strain ϵ defined by

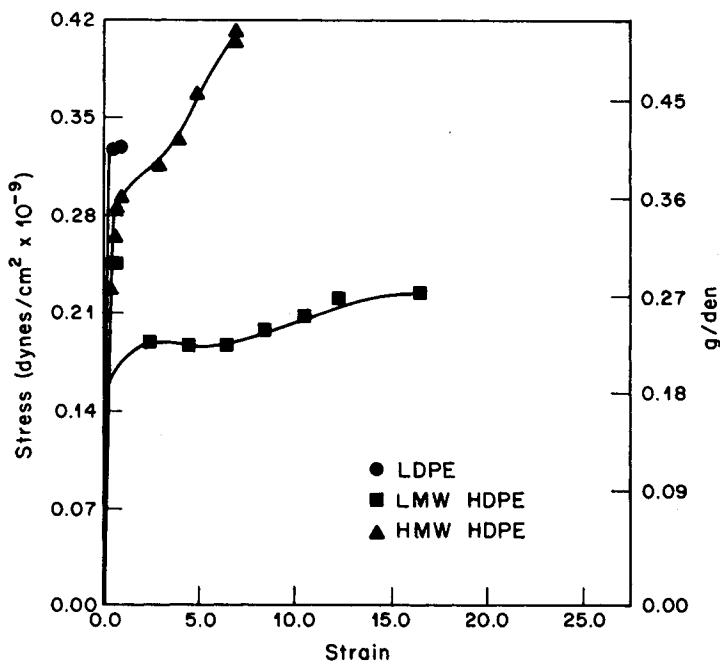$$\sigma = \frac{F}{A_0} \qquad \epsilon = \frac{L - L_0}{L_0} \tag{11a,b}$$

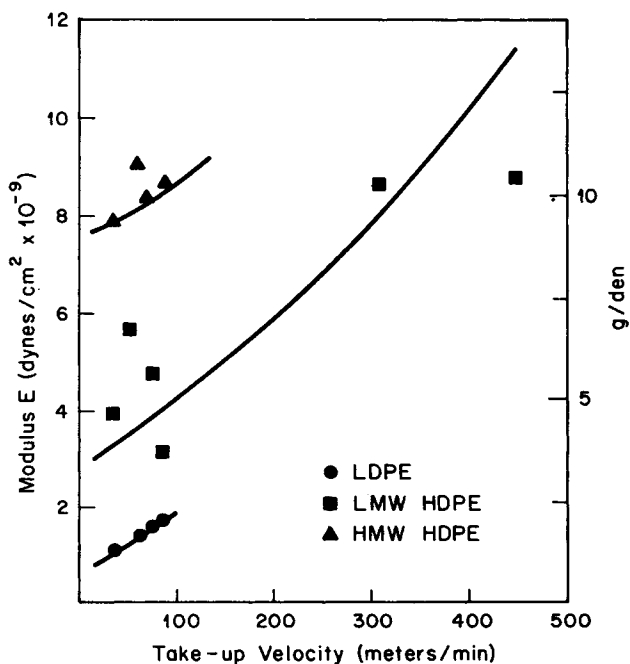Fig. 11. Stress–strain curves for three different polyethylene fibers spun under the same conditions.

Fig. 12. Tangent modulus E for different spun polyethylene fibers as a function of take-up velocity.
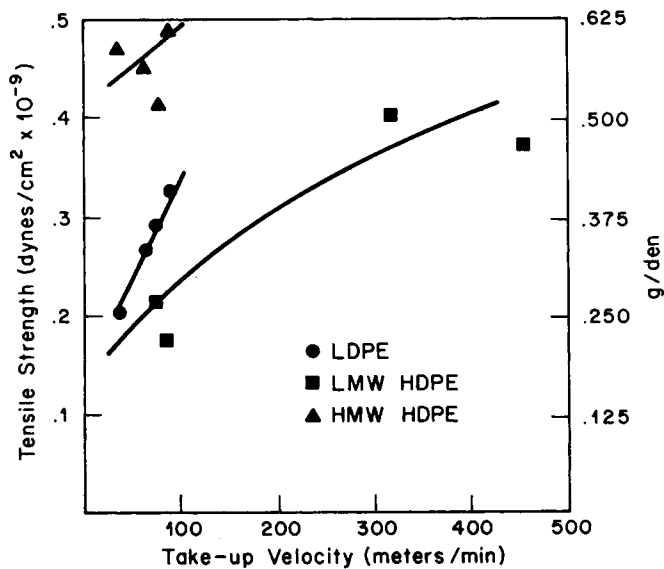
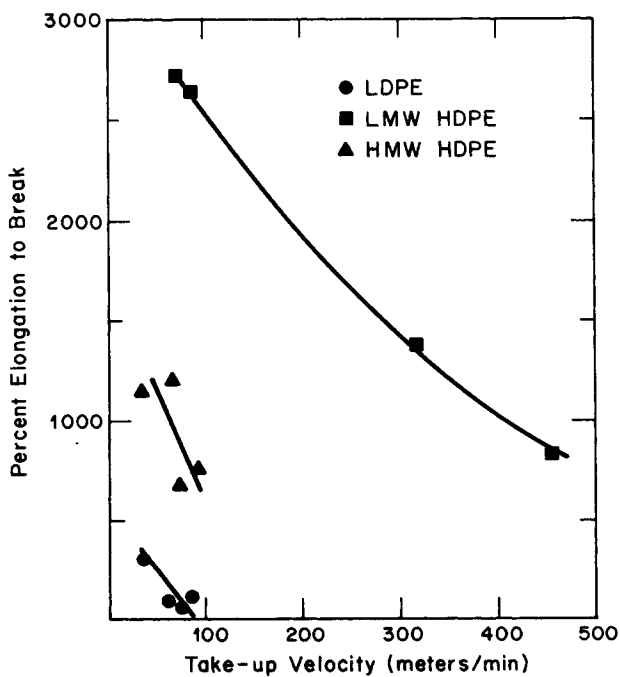Fig. 13. Tensile strength for three different spun polyethylene fibers as a function of take-up velocity.

Fig. 14. Elongation to break for three different spun polyethylene fibers as a function of take-up velocity.

where F is the tensile force, A_0 is the initial cross-sectional area, L is the filament length in the deformed state, and L_0 is the filament length in the initial state. We shall also consider the modulus which is defined as

$$E = \lim_{\epsilon \to 0} \frac{\sigma}{\epsilon}. \tag{11c}$$

Figure 11 contrasts the behavior of the three different polyethylene fibers spun at the same take-up velocity. Figures 12–14 compare modulus E, tensile strength (based upon initial cross-sectional area), and elongation to break for each of the polyethylenes as a function of take-up velocity. The difference in response of the three fibers is striking. The two HDPE's both exhibit necking and longer elongation to break than the LDPE. The HMW-HDPE exhibits higher modulus and tensile stresses than the LMW-HDPE but a smaller elongation to break. In general, increasing the take-up velocity increases the modulus E and the tensile strength but decreases the elongation to break.
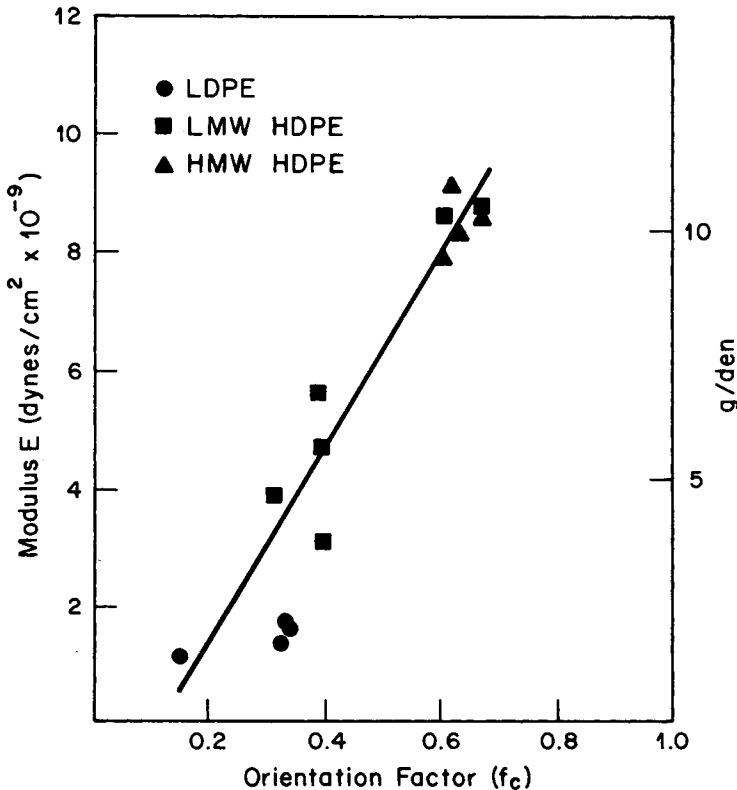

Fig. 15. Tangent modulus E of spun polyethylene fibers as a function of the Hermans orientation factor.
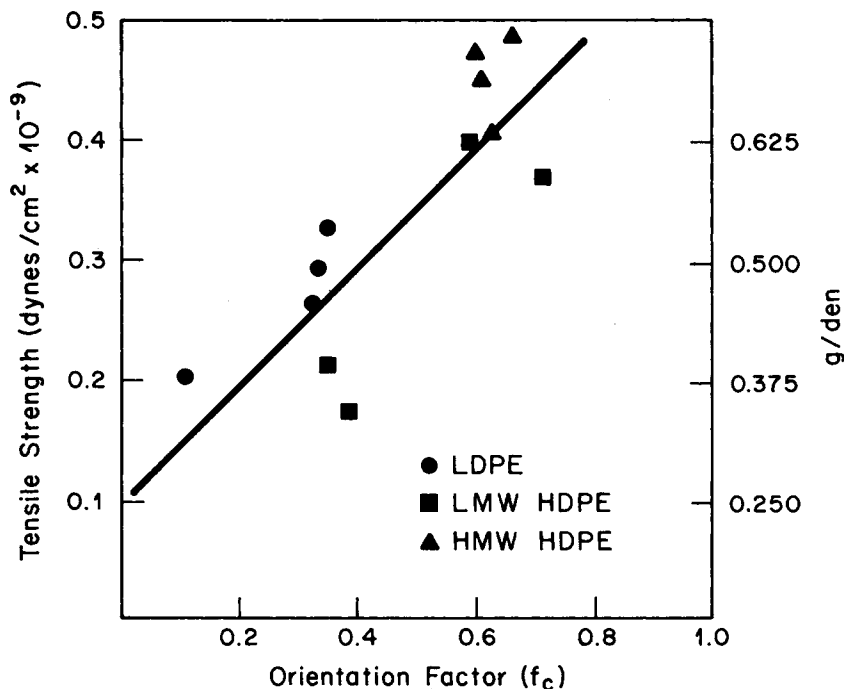
Fig. 16. Tensile strength of spun polyethylene fibers as a function of the Hermans orientation factor.

Discussion of Spun Fiber Data

An attempt was made to correlate the properties of the spun fiber with the level of crystallinity and orientation. For each of the HDPE's, E is a decreasing function of crystallinity X, though only for a small range of crystallinity values. If, however, one introduces LDPE into the picture, the low levels of both E and X relative to that of the HDPE's suggest rather that E is an increasing function of X with considerable variations perhaps due to secondary effects from crystalline orientation and chain length.

Let us now turn to orientation. Samuels[24,26] has correlated mechanical properties in polypropylene with amorphous orientation factors computed from the Stein-Norris equation.[36] However, in view of the results of Dees and Spruiell[18] that the amorphous region seems not to contribute to birefringence in spun high-density polyethylene fibers, it seems better to follow the work of Abbott and White[16] and use the Hermans orientation factor. The uniform variation of E with f_c for all these polyethylenes shown in Figure 15 indicates that crystalline orientation would seem to play a primary role in determining the tensile modulus. A similar attempt was made to correlate tensile strength and elongation to break of the three polyethylenes with the Hermans orientation factor. This is shown in Figures 16 and 17. The data for tensile strength show good correlation.
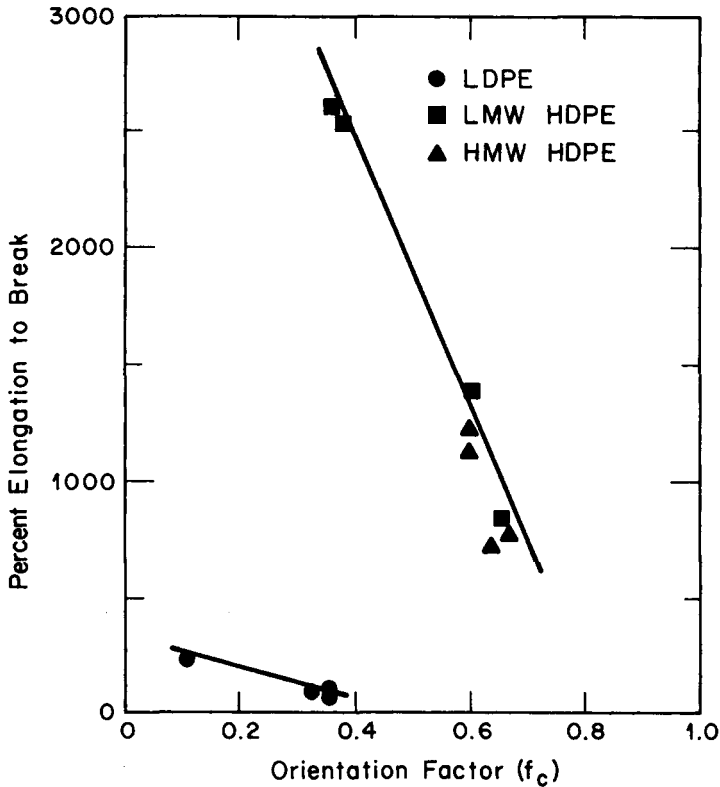
Fig. 17. Elongation to break of spun polyethylene fibers as a function of the Hermans orientation factor.

In contrast, the elongation to break behaviors of the two HDPE's are similar, but that of the LDPE is distinctly different.

Results for Drawn Fibers

Figure 18 compares force–elongation or engineering stress–strain curves for spun and drawn LMW-HDPE with different take-up velocities. The differences are striking. The modulus and tensile strength are found to increase sharply with drawing, while the elongation to break is sharply reduced. The effects are qualitatively similar but more pronounced than the influence of take-up velocity on the mechanical properties of spun fiber.

Interpretation of Drawn Fiber Data

An attempt was made to correlate the tangent modulus, tensile strength, and elongation to break in terms of the Hermans c axis orientation factor. The results are shown in Figures 19–22. Dashed lines separate spun from drawn fibers. It is evident that the modulus and tensile strength (based on initial cross-sectional area) increase slowly and almost linearly to very high
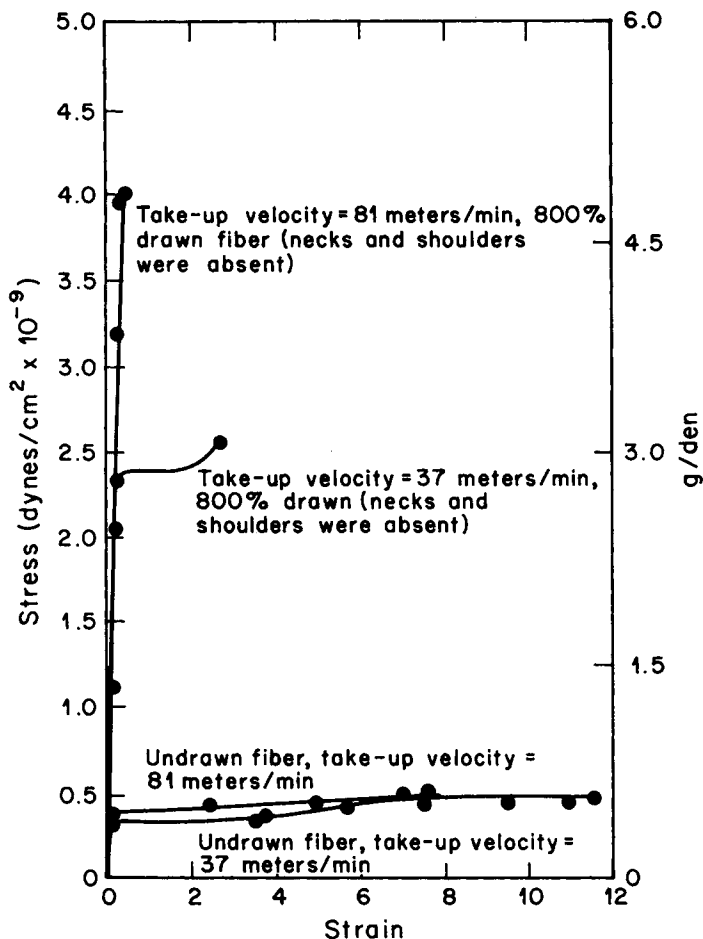
Fig. 18. Comparison of stress–strain curves of spun and drawn fibers taken up at different velocities.

values of f_c followed by an extremely rapid increase. Indeed, it appears that the modulus and tensile strength become independent of orientation at the highest orientation levels.

Figure 21 plots "true" tensile strength based upon final cross-sectional area, determined by

$$\frac{F_b}{A_b} = \frac{F_b}{V_b/L_b} = \frac{V_0}{V_b}\frac{L_b}{L_0}\frac{F_b}{A_0} = \frac{\rho_b}{\rho_0}\frac{L_b}{L_0}\sigma \tag{12}$$

where V and ρ refer to volume and density, and the subscript b, to break. The spun polyethylenes separate into two lines of distinctly different slope, indicating higher levels of true tensile strength for the low-orientation high-density polyethylene fibers.

The question arises as to the maximum possible combination of properties, e.g., tensile strength, achievable by a combined melt spinning–cold
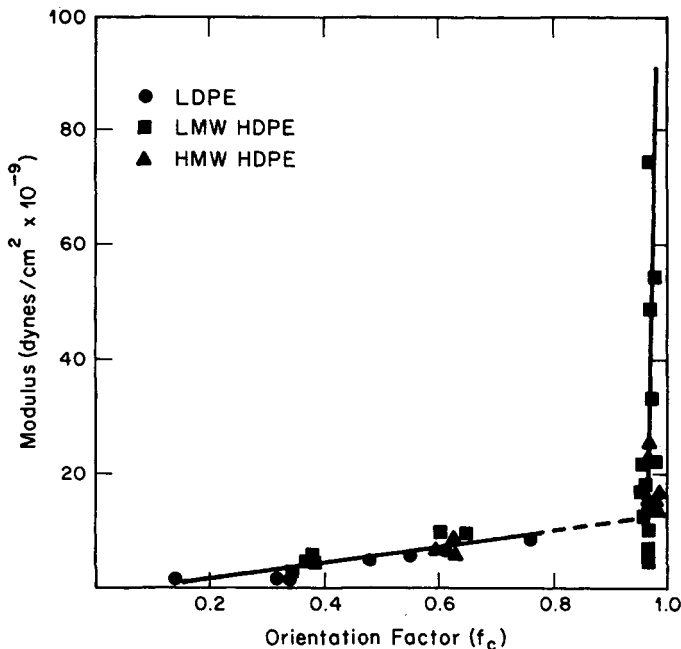
Fig. 19. Tangent modulus E of spun and drawn fibers as a function of Hermans orientation factor.

drawing experiment. It is found by surveying the results of our experiments that if drawing is carried out to the maximum draw ratio, that fibers spun at low take-up velocities have the greatest tensile strength.

INTERPRETATION OF MELT SPINNING AND DRAWING IN TERMS OF CRYSTALLINE MORPHOLOGY

Introduction

A concise discussion of the more detailed structure of crystalline polyethylene would seem worthwhile for future reference. The 100–200 Å repeat distance observed in crystalline polymers led at first to the hypothesis of a "fringed micelle" structure in which polymer chains exist in crystallites of this thickness. It was suggested that a polymer chain might run through several crystallite and interconnecting amorphous regions.[55] However, the discovery of solution-grown thin lamellae of single crystals of polyethylene[55,56] with thicknesses of the same order as this repeat distance led to a considerable rethinking of the crystalline structure of bulk polymers. As a chain-folding hypothesis was necessary to explain the structure of single crystals, it seemed reasonable to apply this to bulk polymers as the x-ray structural data gave no reason to prefer the fringed micelle structure. However, it soon became apparent that the folded-chain lamellae model was able to explain structural features inexplicable by the fringed micelle structure. This was most apparent in the birefringent character of the
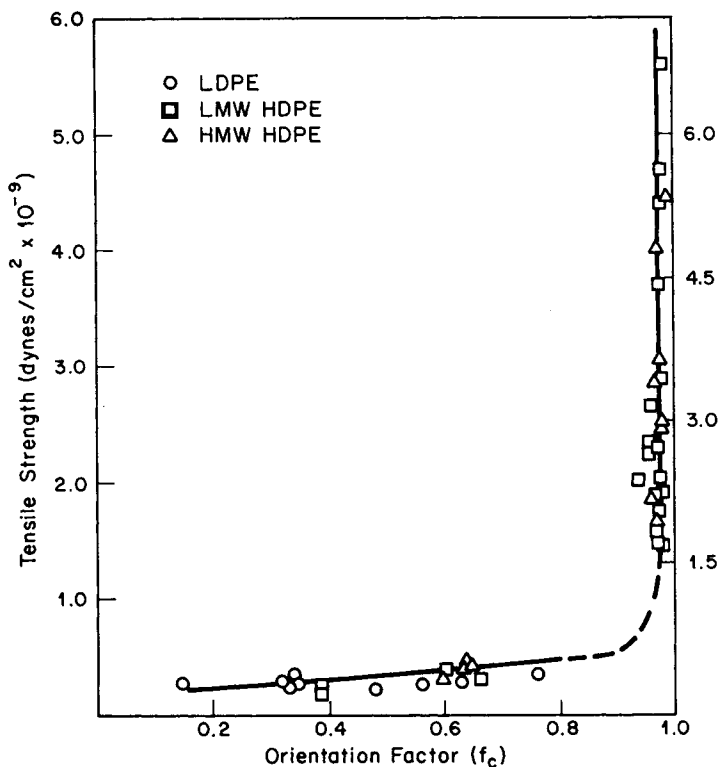
Fig. 20. Tensile strength (based on initial cross-sectional area) of spun and drawn fibers as a function of Hermans orientation factor, in dynes/cm² and grams/denier.

spherulites formed during the bulk crystallization of polyethylene. It has been shown[20,39] that the polymer chain axis must lie in the circumferential direction which is difficult to rationalize in terms of a radially aligned micelle structure. In contrast, this molecular orientation is entirely consistent with a radial growth of folded-chain lamellae. Therefore, we feel the best interpretation of our data on molecular orientation lies in proposing reasonable spatial distributions of folded-chain lamellae. It is not necessary that the chains be regularly folded; indeed, the variation of crystallinity may best be explained in terms of the degree of irregularity in the nature of chain folding, thus creating variations in the amount of "amorphous" material between the lamellae.

Spun Fibers

Spinning of fibers is an important case of crystallization under stress which we have found gives rise to complex molecular orientations in agreement with the observations of many other investigations. Keller and Machin[58] and Clark and Garber,[59] among others, propose that crystallization under low take-up stresses yields "row structures" of folded-chain
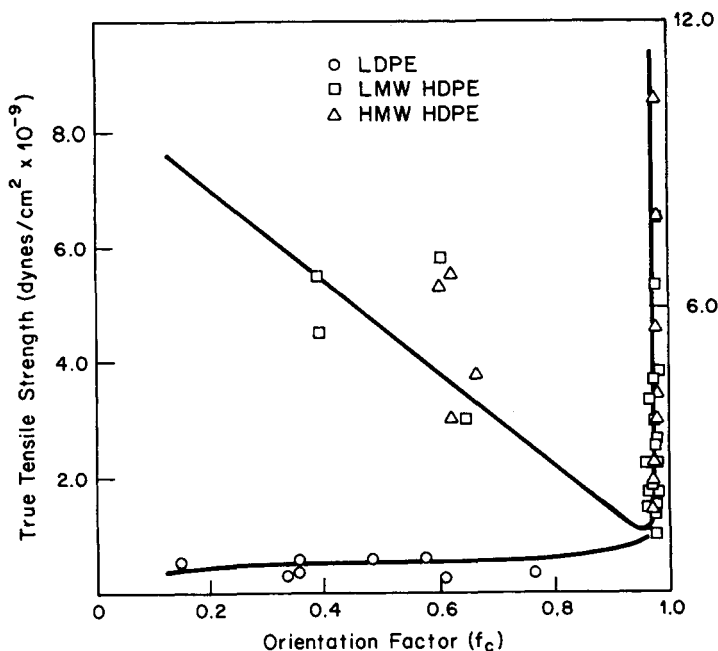
Fig. 21. Tensile strength of spun and drawn fibers (based on final cross-sectional area) as a function of Hermans orientation factor.

lamellae growing from a fibril nucleus. Variations in the amount of twist-ing (a function of stress level) cause wide variations in the nature of the molecular orientation as determined by x-ray diffraction. Katayama, Amano, and Nakamura[11] (developing the ideas of Seto, Hara, Tajima, and Miyagi) consider that lamellae grow perpendicular to the direction of stress and that variations in stress cause corresponding changes in the angle of tilt between the folded-chain stems and the lamella surface. Still another interpretation is offered by Kobayashi and Nagasawa[60] in terms of develop-ment of a conical-shaped spiral structure consisting of lamellae inclined at a constant angle to the stress direction, with the chain stems in turn in-clined to the lamella surface.

It seems quite impossible for us to distinguish uniquely between these various models. However, we offer what appears to us to be the most reasonable interpretation of our data. Common to all of the cases of spun fibers studied is the orientation of the b axis perpendicular to the direction of stress. Superimposed on this is a rather large variation in the orienta-tions of the a and c axes. These data, summarized in Figure 6, are most easily explained by the twisted lamella hypothesis. In spherulites of polyethylene, lamellae grow parallel to the unit-cell b axis.[61] Thus, the b axis is parallel to the spherulite radius. Under stress, as in fiber spinning, we propose, in agreement with the interpretations of Keller and Machin,[58] that a fundamental change in nucleation occurs. In a region of localized,
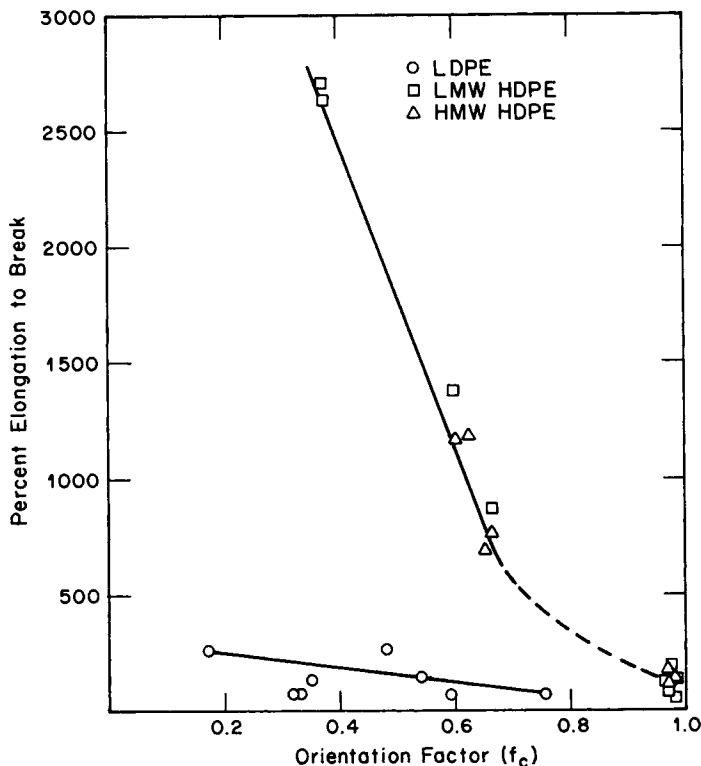
Fig. 22. Elongation to break of spun and drawn fibers as a function of Hermans orientation factor.

high extensional flow, a fibril nucleus is created, which is not necessarily an extended chain structure but creates a *row* of nucleation sites parallel to the stress direction from which lamellae grow in a manner similar to that from the "point" nucleus of the spherulite. If the growth axis of the lamellae is parallel to the b axis as in the spherulite, the b axis of the row structure will be normal to the fiber axis. As growth of the lamellae continues, variations in the degree of twisting about the b axis may occur. Growth of this type gives a Hermans-Stein orientation function of $f_b = -0.5$, whatever the degree of twist. In the limiting case of full 360° twisting of lamellae about the growth direction in a row structure, it follows that the three orientation functions must be

$$f_b = -0.5 \qquad f_a = f_c = 0.25. \tag{13}$$

In another limiting case of lamellae growth in a row structure but with no twisting,

$$f_b = f_a = -0.5 \qquad f_c = 1.0. \tag{14}$$

Our interpretation of the data in Figure 6 is that in the case of LDPE, at low take-up velocities (low stress), the lamellae have a high degree of twist-

ing, perhaps in an irregular manner as suggested by the study of LDPE spherulites by Geil.[62] At higher stresses, the lowering of f_a and corresponding increase in f_c suggest less twisting, although the low value of f_c at the limits of spinnability implies a substantial degree of twisting is still present.

The LMW-HDPE seems to follow a similar progression of structural changes with increasing take-up velocities. In this case, the tendency of the lamellae to twist is less than in the LDPE. The LMW-HDPE structures approach the row structure of untwisted lamellae as expressed by eq. (14). The higher molecular weight specimen of HDPE shows no evidence of f_a having a positive value, implying a pronounced tendency for planar conformation of lamellae. As we have seen, planarity in lamella growth is associated with a high stress level during crystallization. It is possible that as a result of greater molecular entanglement at high molecular weight, the stress level, even at low take-up velocities, is sufficiently high to prevent development of twisted lamellae. We must also consider the possibility that the two curves of HDPE may be similar in nature but displaced along the axis of take-up velocity. That is, data recorded at very low take-up velocities for HMW-HDPE might show a region of positive f_a similar to that of LMW-HDPE.

It is significant to note that in our interpretation of morphology of melt-spun fibers of polyethylene, the complex orientation functions are attributed solely to variations in the conformation and orientation of lamellae and not to break-up and unfolding of lamellae. We restrict these morphologic phenomena to postdrawing operations as described in the next section.

Drawn Fibers

The great increases in modulus and tensile strength and decrease in elongation to break associated with the drawing of fibers clearly imply a disruption of the basic (folded-chain lamellae) morphology. Indeed, the changes in mechanical properties are no longer directly correlatable in terms of averaged orientations. Enormous increases in modulus and tensile strength occur while f_a, f_b, and f_c remain unchanged. Various views of these deformation mechanisms have been summarized by Peterlin and his associates[23,63,64] and others.

Basically, these ideas can be summarized as follows: Initially, the undrawn crystalline polymer consists of folded-chain lamellae joined by a small but important fraction of tie molecules. On drawing, the lamellae break up into folded-chain blocks, on the order of 100–300 Å in diameter, which subsequently aggregate to form the fundamental unit of drawn structure—the fibril. The fibril consists of alternating crystal blocks (small chain-folded units) and amorphous regions. The latter consists of chain folds, free chain ends, and tie molecules. Thus, the folded-chain blocks which were neighbors laterally in the undeformed structure become neighbors longitudinally in the drawn fibril. Tie molecules which connect the blocks in the longitudinal (draw) direction provide the principal source for strength and modulus of the fiber. According to this model, the tensile strength and modulus will increase with the fraction of the tie molecules.

References

1. W. H. Carothers and J. W. Hill, *J. Amer. Chem. Soc.*, **54**, 1579 (1932).

2. W. H. Carothers and F. J. Van Natta, *J. Amer. Chem. Soc.*, **55**, 4714 (1933).

3. E. K. Bolton, *Ind. Eng. Chem.*, **34**, 53 (1942).

4. A. Keller, *J. Polym. Sci.*, **21**, 363 (1956).

5. A. Ziabicki and K. Kedzierska, *J. Appl. Polym. Sci.*, **2**, 14 (1959).

6. A. Ziabicki and K. Kedzierska, *J. Appl. Polym. Sci.*, **6**, 111 (1962).

7. A. Ziabicki and K. Kedzierska, *J. Appl. Polym. Sci.*, **6**, 361 (1962).

8. A. B. Thompson, in *Fibre Structure*, J. W. S. Hearle and R. H. Peters, Eds., Butterworth, Textile Institute, London, 1963.

9. T. D. Higgins and G. M. Bryant, *J. Appl. Polym. Sci.*, **8**, 2399 (1964).

10. A. Ziabicki, in *Man-Made Fibers*, Vol. I, H. Mark, S. M. Atlas, and E. Cernia, Eds., Wiley, New York, 1967.

11. K. Katayama, T. Amano, and K. Nakamura, *Kolloid Z.-Z. Polym.* **226**, 125 (1968).

12. T. Ishibashi, K. Aoki, and T. Ishii, *J. Appl. Polym. Sci.*, **14**, 1597 (1970).

13. P. Y. E. Fung and S. H. Carr, *Macromol. Sci. Phys.*, **B6**, 621 (1972).

14. T. Kitao, S. Ohya, J. Furukawa, and S. Yamashita, *J. Polym. Sci. (Polym. Phys.,)* **11**, 1091 (1973).

15. K. Katayama and T. Amano, *Appl. Polym. Symp.*, **20**, 237 (1973).

16. L. E. Abbott and J. L. White, *Appl. Polym. Symp.*, **20**, 247 (1973).

17. A. Peterlin, *Appl. Polym. Symp.*, **20**, 269 (1973).

18. J. R. Dees, and J. E. Spruiell, *J. Appl. Polym. Sci.*, **18**, 1053 (1974).

19. I. Fankuchen and H. Mark, *J. Appl. Phys.*, **15**, 364 (1944); M. E. Bergmann, I. Frankuchen, and H. Mark, *Text. Res. J.*, **18**, 1 (1948).

20. C. W. Bunn and T. C. Alcock, *Trans. Faraday Soc.*, **41**, 317 (1945).

21. P. I. Vincent, *Polymer*, **1**, 7 (1960).

22. N. Kasai and M. Kakudo, *J. Polym. Sci.*, **A2**, 1955 (1964).

23. A. Peterlin, in *Man-Made Fibers*, Vol. I., H. Mark, S. M. Atlas, and E. Cernia, Eds., Wiley, New York, 1967.

24. R. J. Samuels, *J. Polym. Sci. A-2*, **6**, 2021 (1968); *J. Macromol. Sci.*, **B4**, 701 (1970).

25. J. D. Muzzy and D. Hansen, *Text. Res. J.*, **41**, 436 (1971).

26. R. J. Samuels, *J. Polym. Sci. A-2*, **10**, 781 (1972).

27. D. Acierno, J. N. Dalton, J. M. Rodriguez, and J. L. White, *J. Appl. Polym. Sci.*, **15**, 2395 (1971).

28. I. J. Chen, G. E. Hagler, L. E. Abbott, D. C. Bogue, and J. L. White, *Trans. Soc. Rheol.* **16**, 473 (1972).

29. J. E. Spruiell, D. E. McCord, and R. A. Beuerlein, *Trans. Soc. Rheol.*, **16**, 535 (1972).

30. J. J. Hermans, P. H. Hermans, D. Vermaas, and A. Weidinger, *Rec. Trav. Chim.*, **65**, 427 (1946).

31. R. S. Stein, *J. Polym. Sci.*, **31**, 327 (1958).

32. L. E. Alexander, *X-Ray Diffraction Methods in Polymer Science*, Wiley-Interscience, New York, 1969.

33. C. W. Bunn, *Trans. Faraday Soc.*, **35**, 482 (1939).

34. S. Kavesh and J. M. Schultz, *Polym. Eng. Sci.*, **9**, 452 (1969).

35. A. Ziabicki, *J. Appl. Polym. Sci.*, **2**, 24 (1959).

36. R. S. Stein and F. H. Norris, *J. Polym. Sci.*, **16**, 381 (1956).

37. Samuels, R. J. in *The Science and Technology of Polymer Films*, Vol. I, O. J. Sweeting, Eds., Interscience, New York, 1968.

38. E. W. Fischer and G. F. Schmidt, *Angew. Chem.*, **74**, 551 (1962).

39. W. M. D. Bryant, *J. Polym. Sci.*, **2**, 547 (1947).

40. R. S. Stein, *J. Polym. Sci. C*, **15**, 185 (1966).

41. M. E. Morrison, *A.I.C.h.E.J.*, **16**, 57 (1970).

42. R. D. Van Veld, G. Morris, and H. R. Billica, *J. Appl. Polym. Sci.*, **12**, 2700 (1968).

43. W. M. Pasika, A. C. West, and E. L. Thurston, *J. Polym. Sci. (Polym. Phys.)*, **10**, 2313 (1972).

44. T. F. Ballenger, I. J. Chen, G. E. Hagler, D. C. Bogue, and J. L. White, *Trans. Soc. Rheol.* **15**, 195 (1971).

45. S. Middleman, *The Flow of High Polymers*, Interscience, New York, 1968.

46. L. H. Tung and W. C. Taylor, *J. Polym. Sci.*, **21**, 144 (1956).

47. P. R. Swan, *J. Polym. Sci.*, **42**, 525 (1960).

48. Lord Rayleigh, *Proc. London Math. Soc.*, **10**, 4 (1879).

49. Lord Rayleigh, *Phil. Mag.*, **34**, 145 (1892).

50. S. Tomotika, *Proc. Roy. Soc.*, **A153**, 302 (1936).

51. J. R. A. Pearson and M. A. Matovich, *Ind. Eng. Chem., Fundam.*, **8**, 605 (1969).

52. H. Chang and A. S. Lodge, *Rheol. Acta*, **10**, 448 (1971).

53. M. Reiner, *Deformation and Flow*, Lewis, London, 1948.

54. J. E. Spruiell, personal communication, 1972–73.

55. K. Herman, O. Gerngross, and W. Abitz, *Z. Phys. Chem.*, **B10**, 371 (1930).

56. P. H. Till, *J. Polym. Sci.*, **24**, 361 (1957).

57. A. Keller, *Phil. Mag.*, **2**(8), 1171 (1957).

58. A. Keller and M. J. Machin, *J. Macromol. Sci. Phys.*, **B1**, 47 (1967).

59. E. S. Clark and C. A. Garber, *Int. J. Polym. Mat.*, **1**, 31 (1971).

60. K. Kobayashi and T. Nagasawa, *J. Polym. Sci.*, **C15**, 163 (1966).

61. A. Keller, *J. Polym. Sci.*, **17**, 291 351 (1955).

62. P. H. Geil, *J. Polym. Sci.*, **51**, S10 (1961).

63. G. Meinel, N. Morosoff, and A. Peterlin, *J. Polym. Sci. A-2*, **8**, 1723 (1970).

64. G. Meinel and A. Peterlin, *J. Polym. Sci. A-2*, **9** 67 (1971).